2010

SnO2-NiO-C nanocomposite as a high capacity anode material for lithium-ion batteries

Mohd Faiz Hassan
University of Wollongong, mfh125@uow.edu.au

Md Mokhlesur Rahman
mrahman@uow.edu.au

Zaiping Guo
University of Wollongong, zguo@uow.edu.au

Zhixin Chen
University of Wollongong, zchen@uow.edu.au

Hua Liu
University of Wollongong, hua@uow.edu.au

Publication Details

Hassan, M., Rahman, M. M., Guo, Z., Chen, Z. & Liu, H. (2010). SnO_2-NiO-C nanocomposite as a high capacity anode material for lithium-ion batteries. Journal of Materials Chemistry, 20 (43), 9707-9712.

SnO_2–NiO–C nanocomposite as a high capacity anode material for lithium-ion batteries†

Mohd Faiz Hassan,[ab] M. M. Rahman,[a] Zaiping Guo,*[ac] Zhixin Chen[c] and Huakun Liu[a]

Received 6th May 2010, Accepted 17th August 2010
DOI: 10.1039/c0jm01341b

Carbon-coated SnO_2–NiO nanocomposite was successfully synthesized *via* the molten salt route, using $SnCl_2 \cdot H_2O$ and $NiCl_2 \cdot 6H_2O$ as the starting materials, with a molten salt composition of H_2O_2 : $LiOH \cdot H_2O$: $LiNO_3$ as a solvent at 300 °C. The synthesis was followed by a carbon layering process. The phases and morphology of the as-prepared samples were examined by X-ray diffraction and transmission electron microscopy. Electrochemical investigation was carried out by using a series of complementary techniques, including galvanostatic charge–discharge, cyclic voltammetry, and impedance spectroscopy. The results confirmed that the carbon-coated SnO_2–NiO nanocomposite has higher discharge capacity, better rate capability, and excellent cycling performance in comparison to the uncoated SnO_2–NiO nanocomposite. The carbon-coated SnO_2–NiO nanocomposite electrode exhibited a reversible capacity of about 529 mA h g^{-1} at 800 mA g^{-1}, and 265 mA h g^{-1} at 1600 mA g^{-1}, even after 500 cycles. The excellent electrochemical performance of the SnO_2–NiO–C nanocomposite can be mainly attributed to the combined effects of the nanostructure, the carbon layering on the SnO_2 and NiO nanoparticles, and the ultra-fine carbon matrix, because the three factors would contribute to high electronic conductivity, reduce the traverse time of electrons and lithium ions, and also prevent high volume expansion during cycling. Due to its excellent electrochemical performance, the SnO_2–NiO–C nanocomposite could be considered as a promising anode material for future lithium-ion batteries to be used in electric vehicles and hybrid electric vehicles.

Introduction

Research and development on lithium-ion batteries as portable power sources are continuing to attract more and more attention. Lithium-ion batteries have become a very topical research area in science and industry due to their high-energy storage density, long cycle life, and capacity to act as high power sources.[1,2] However, the main challenge in the fabrication of these batteries is to ensure that the electrodes maintain their integrity during hundreds of discharge–recharge cycles. Many recently proposed electrode systems have limited cycle life due to the growth of passivation layers and/or Li-alloying agglomeration, which leads to high capacity loss and poor cycling performance, thus restricting their application as anode materials for lithium ion batteries.[3,4] To improve electrode capacity, cycling performance, and rate capability, some hybrid materials with multidimensional networks characterized by high surface area, high conductivity, and highly porous nanostructures have been developed.[5–7] Recently, stannous oxide (SnO_2) has been intensively studied as an active material in hybrid systems. Its high theoretical storage capacity of 782 mA h g^{-1} and maximum intake of 4.4 Li per Sn atom to form $Li_{4.4}Sn$ during alloying make it one of the most suitable compounds to replace carbon anode in the lithium ion battery. However, tin-based materials have a disadvantage, in that they undergo significant volume expansion and contraction during lithium intercalation and de-intercalation.[8,9] This causes cracking and crumbling, and results in "dead volume", which is electrically disconnected from the bulk material or the current collector. The mechanically inactive "dead volume" results in subsequent degradation of electrode performance during cycling. Special structures have been designed to stabilize the morphology of electrodes in order to alleviate the volume changes and mechanical stress in Sn-metal alloy[10–14] or tin-based composite.[15–17]

In such cases, another inactive or less active composition is used as a supporting and conducting matrix to buffer the volume change. Many of these new anode materials are composed of Sn or SnO_2 in combination with other metal oxides, such as ZnO–SnO_2,[18] RuO_2–SnO_2,[19] $CuFe_2O_4$–SnO_2,[20] SiO_2–SnO_y,[21] CuO(nanotube)–SnO_2,[22] Sn–Co–C,[23] and Sn–Ni–C.[24] These hybrid systems have some properties which would be difficult to achieve in a single system, such as higher catalytic activity, capability to absorb the volume variation of the active material during lithium insertion, and ability to react reversibly with a larger amount of lithium, so that they can greatly improve the electrochemical performance compared to the single systems.[18,21,25–27] However, studies on SnO_2–NiO and carbon-coated SnO_2–NiO as anode materials for lithium-ion batteries have been rarely reported.

[a]*Institute for Superconducting and Electronic Materials, University of Wollongong, New South Wales, 2522, Australia. E-mail: zguo@uow.edu.au; Fax: +61-2-4221-5731; Tel: +61-2-4221-5225*
[b]*Department of Sciences Physics, University Malaysia Terengganu, Kuala Terengganu, 21030, Malaysia*
[c]*School of Mechanical, Mechatronic and Materials Engineering, University of Wollongong, New South Wales, 2522, Australia*

† Electronic supplementary information (ESI) available: TGA results for SnO_2–NiO and SnO_2–NiO–C samples, TEM images of individual SnO_2 (a) and NiO (b) powders, with the magnified insets showing the corresponding *d*-spacing values, and TEM images of SnO_2–NiO and SnO_2–NiO–C powders at different magnifications. See DOI: 10.1039/c0jm01341b

In this study, carbon-coated SnO_2–NiO nanocomposite was synthesized by a simple molten salt technique followed by a carbon layering process. SnO_2–NiO particles were simply and effectively coated by amorphous carbon obtained from malic acid dispersed in toluene. By using this method, we avoided the usual drastic volume variation and agglomeration of nanoparticles, and enhanced the kinetic properties of the active materials. Consequently, the electrochemical performance of the electrode was significantly improved. Furthermore, the molten salt method is easy to carry out and scale up, the treatment temperature is low, and the raw molten salt materials are recyclable, as we reported in our previous work.[28] In this investigation, the structural and electrochemical properties of the SnO_2–NiO–C nanocomposite are characterized with the aim of obtaining better anode materials for lithium-ion batteries.

Experimental

Material preparation

Commercial lithium hydroxide monohydrate (Aldrich), lithium nitrate (Aldrich), hydrogen peroxide (Sigma-Aldrich), tin(II) chloride dihydrate (Analar-BDH), and nickel(II) chloride hexahydrate ((Sigma-Aldrich) were used as received. 100 mmol of lithium nitrate, 100 mmol of lithium hydroxide monohydrate, 10 mmol of tin(II) chloride dehydrate, and 10 mmol of nickel(II) chloride hexahydrate were mixed in an agate mortar to obtain a homogenous composition. Then, 50 mmol of hydrogen peroxide were added into the mixture and stirred for 3 h. The mixture was then heated at 120 °C for 4 h in a vacuum oven, followed by a further heat-treatment in air at 300 °C for 3 h in a muffle furnace. After cooling naturally in air, the SnO_2–NiO composite was separated from the eutectic mixture by washing with a large amount of de-ionized (DI) water and by centrifugation. The product, the bare SnO_2–NiO, was then dried under vacuum at 100 °C overnight to remove the residual water. The amorphous carbon coated SnO_2–NiO nanopowder was prepared by a surface coating method. Toluene (C_7H_8, 99.5%) and malic acid ($C_4H_6O_5$, 99%) were used as the solvent and the carbon source, respectively, during the coating process. Both SnO_2–NiO and malic acid were dispersed together in toluene with continuous stirring for 2 h at room temperature. The slurry was dried at 150 °C for 6 h at a pressure of 0.1 MPa and then further heat-treated at 300 °C for 3 h in air. The resultant powders were collected, washed, and vacuum-treated again at 120 °C for 24 h to eliminate residual water on the powder surfaces.

Material characterization

X-Ray diffraction analysis (XRD) was carried out on the synthesized powders using a GBC MMA diffractometer with Cu Kα radiation and a graphite monochromator. Raman spectroscopy was conducted using a Jobin Yvon HR800 to identify the amorphous carbon in the composite powder. Thermogravimetric analysis (TGA) was performed on a SETARAM Thermogravimetric Analyzer (France) in air to determine the changes in sample weight with increasing temperature and to estimate the amount of carbon present in the SnO_2–NiO nanocomposite. Transmission electron microscopy (TEM) was performed using a 200 kV JEOL 2011 instrument equipped with a JEOL-Energy Dispersive X-ray Spectrometer (EDS). TEM powder samples were prepared by dispersion onto holey carbon support films. The as-prepared powders were used to prepare electrodes by dispersing 75 wt% active materials with 20 wt% of acetylene black, and 5 wt% of poly(vinylidene fluoride) (PVDF) binder in 1-methyl-2-pyrrolidinone (NMP) solvent. The mixture was then ground until it became homogeneous. The resulting slurry was pasted onto copper foil and dried in a vacuum oven at 120 °C for 12 h to remove the NMP solvent, and the electrodes were then pressed under a pressure of approximately 200 kg cm^{-2}. The cells were assembled in an argon-filled glove box (H_2O, O_2 < 0.1 ppm, Mbraun, Unilab, USA). The electrolyte was 1 M $LiPF_6$ in a mixture of ethylene carbonate (EC) and dimethyl carbonate (DMC) (1 : 1 by volume, provided by MERCK KgaA, Germany), and microporous polypropylene film was used as the separator. The cells were galvanostatically discharged and charged in the voltage range of 0.01–3.0 V *vs.* Li/Li$^+$. Cyclic voltammetry (CV) measurements were performed using an electrochemical workstation (CHI660A) at a scan rate of 0.1 mV s^{-1} between 0.01 and 3.0 V *versus* Li/Li$^+$. Impedance measurements were carried out several times with a computer controlled CHI instrument at room temperature (RT). The frequency range was varied from 1 MHz to 10 mHz with ac signal amplitude of 10 mV. The collected data were analyzed using ZPlot® and ZView™ software to obtain the Nyquist plots (Z' *vs.* $-Z''$).

Results and discussion

The molten salt compositions with their low melting point are helpful in hindering the growth of SnO_2–NiO particles in a eutectic environment. The method shows an accelerated reaction rate and controllable particle morphology, because the salt melt acts as a strong solvent with a high ionic diffusion rate.[29] Furthermore, the amorphous carbon obtained by the present carbon-layering process, among other modes of action, suppresses aggregation of nanoparticles and thus generates porous SnO_2–NiO–C nanostructures. The overall synthetic procedure is schematically described in Scheme 1.

The Raman spectrum of the SnO_2–NiO–C composite is shown in Fig. 1. The results exhibit two kinds of peaks, namely, the

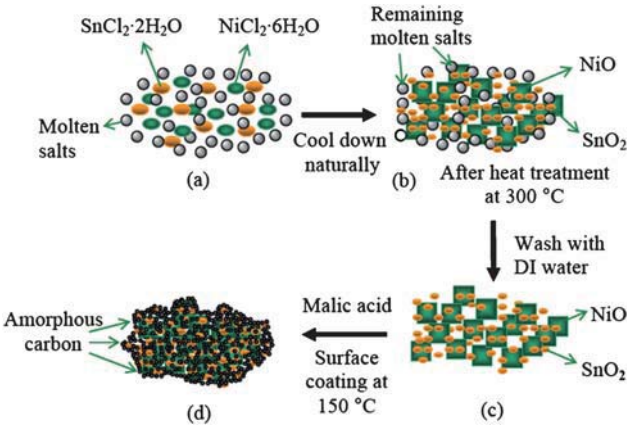

Scheme 1 Schematic model of synthetic procedure: (a) mixed raw materials; (b) solid molten salts and SnO_2–NiO; (c) un-coated SnO_2–NiO composite; and (d) final product of SnO_2–NiO–C.

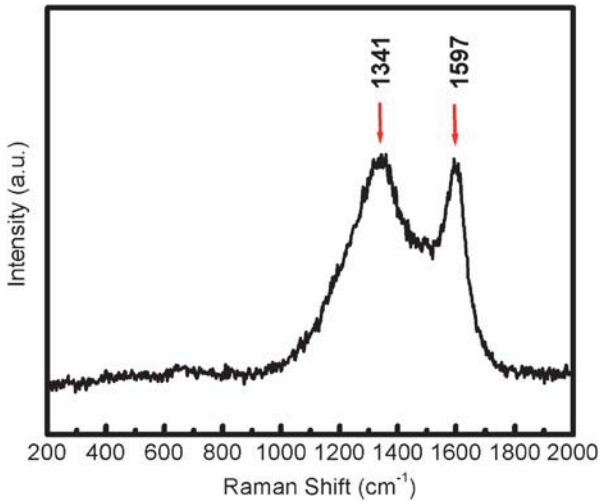

Fig. 1 Raman spectrum of the SnO_2–NiO–C nanocomposite powder.

graphite carbon peak (G peak) located at ~1597 cm^{-1} and the disordered carbon peak (D peak) at ~1341 cm^{-1}. Thus, it confirms that the carbon in the composite is amorphous carbon.[30–32] Fig. 2 presents the X-ray diffraction patterns of the coated and uncoated compounds, which were obtained using a scan rate of 2° per min in the range of 10–80°. Both diffraction patterns clearly show that there is a two-phase structure, where some peaks are broad and have low intensity, and the others are sharp and have relatively high intensities. The broad reflection peaks can be easily indexed to a tetragonal phase of cassiterite SnO_2 (JCPDS 2-1340, space group *P*42/*mnm* (no. 136)), while the sharp reflection peaks can be indexed as a cubic phase of bunsenite NiO (JCPDS 71-1179, space group *Fm*3*m* (no. 225)). The approximate crystallite sizes in the powders were estimated to be 1–2 nm for the SnO_2 and 13–90 nm for the NiO, respectively, using the Debye–Scherrer equation, where (1 0 1) was used for SnO_2 and (2 0 0) for NiO, with the Si standard (2 2 0) peak used as a reference. Broad diffraction peaks or lines corresponding to amorphous or crystalline carbon were of insufficient intensity to be detected against the background in the XRD pattern of the

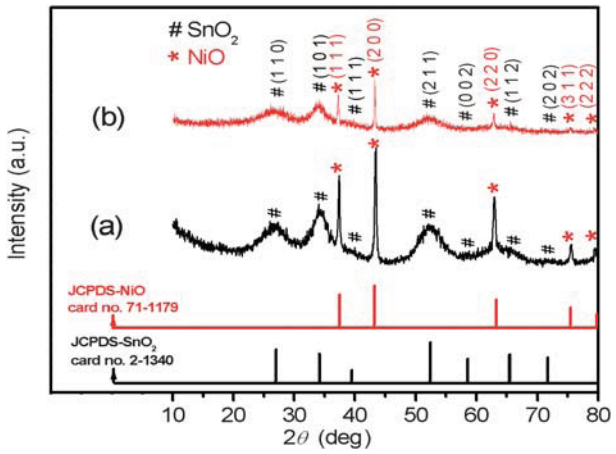

Fig. 2 XRD patterns of the (a) as-prepared SnO_2–NiO and (b) SnO_2–NiO–C powders.

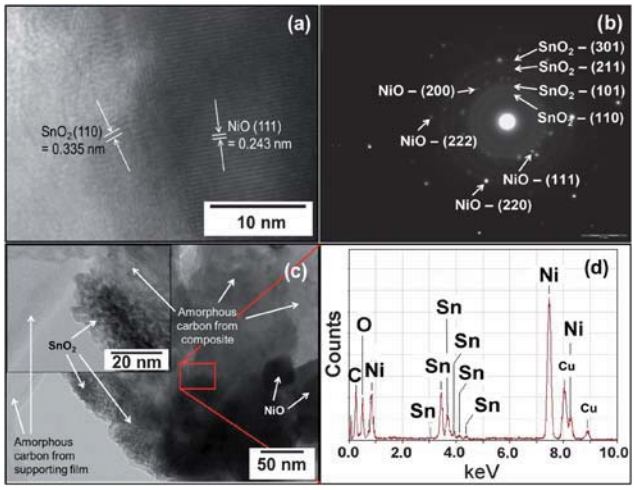

Fig. 3 TEM image of SnO_2–NiO powder (a), corresponding SAED pattern (b), TEM image of SnO_2–NiO–C powder (inset: the image scale at 20 nm) (c), and corresponding EDS spectrum of the marked region of (d).

SnO_2–NiO–C composite, however, amorphous carbon in the composite product was detected by TGA, as shown in Fig. S1 of the ESI† and by TEM examination. From comparison with the Joint Committee on Powder Diffraction Standards (JCPDS) database lines in the figure, no other peaks were detected, even after the surface coating, which indicates that SnO_2–NiO and carbon-coated SnO_2–NiO nanocomposites were successfully obtained under the current synthetic conditions.

Transmission electron microscope (TEM) images of the SnO_2–NiO and SnO_2–NiO–C powders are shown in Fig. 3. Fig. 3(a) presents a TEM image of the SnO_2–NiO powder. This high resolution TEM image of the SnO_2–NiO shows that the interplanar spacing of individual particles in the SnO_2 (110) and the NiO (111) directions is approximately 0.335 and 0.243 nm between neighbouring planes. The individual particles of SnO_2 and NiO in the composite samples matched well with SnO_2 and NiO particles which are synthesised separately (Fig. S2†). Meanwhile, the crystallite sizes of individual particles of SnO_2 and NiO are in the range of 1–2 nm and 13–90 nm, respectively, which are in good agreement with the values from the Scherrer calculations. The values of the crystal sizes along three crystallographic directions for the SnO_2–NiO and SnO_2–NiO–C samples are shown in Table S1 in the ESI†. Fig. 3(b) contains the corresponding selected area electron diffraction (SAED) pattern of the SnO_2–NiO powder. The diffraction rings and discrete spots are due to the very fine SnO_2 and relatively coarse NiO particles, respectively. Therefore, this diffraction pattern can be indexed as mixed SnO_2 and NiO. The result is not only consistent with the XRD results presented above, but also with the TEM image of the SnO_2–NiO–C in Fig. 3(c), which shows that the powder consists of large NiO and small SnO_2 particles, as well as amorphous carbon. It should be noted here that the amorphous carbon was successfully identified by comparing it with the amorphous carbon on the copper grid, as observed in the inset of Fig. 3(c). The EDS spectrum obtained from the marked region of Fig. 3(c) is given in Fig. 3(d). The Sn L peaks come from the SnO_2, the Ni K and L peaks from NiO, the O K peak from the

both NiO and SnO_2, the C K peak from the carbon coating, and the Cu K and L peaks from the Cu grid. It was noted that after layering with amorphous carbon, the structure of SnO_2–NiO clearly indicated the order of each element to be better, neat and orderly (Fig. S3†).

Electrochemical performances of the SnO_2–NiO and SnO_2–NiO–C electrodes are presented in Fig. 4. Fig. 4(a) shows cyclic voltammograms obtained in the potential range of 3.0–0.01 V and collected at a sweep rate of 0.1 mA s^{-1}. Several reduction and oxidation peaks could be observed in the CV results, implying that the samples have a multiple reaction mechanism, which could be characterized by the following equations:

$$2Li^+ + NiO + 2e^- \Leftrightarrow Ni + Li_2O \quad (1)$$

$$4Li^+ + SnO_2 + 4e^- \Rightarrow Sn + 2Li_2O \quad (2)$$

$$4.4Li^+ + Sn + 4.4e^- \Leftrightarrow Li_{4.4}Sn \quad (3)$$

$$xLi^+ + C\ (\text{amorphous carbon}) + xe^- \Leftrightarrow Li_xC \quad (4)$$

NiO has been proposed[3] to have a one-step reaction with lithium, as expressed in eqn (1). As observed in the reduction process, the peak located at 0.95 V corresponds to the reduction process of NiO into Ni, and the formation of amorphous Li_2O and the solid electrolyte interphase (SEI). The two oxidation peaks of NiO positioned at 1.58 and 2.2 V could be related to the decomposition of the SEI and Li_2O, and the formation of NiO, which is fully reversible, according to the reaction of eqn (1).[33,34] Meanwhile, SnO_2 is well known to have a two-step reaction, as expressed in eqn (2) and (3).[35] In the first step reaction, the peaks positioned at 0.66 and 0.35 V correspond to the reduction reaction of SnO_2 with lithium ions to form metallic Sn and Li_2O (eqn (2)). The oxidation peaks observed at 0.55 and 1.28 V can be related to the reaction between metallic Sn and lithium ions to form Li_xSn (eqn (3)). Only this third reaction took place for the next oxidation/reduction process.[36,37] It might be believed that the amorphous carbon participates in the electrochemical reaction as expressed in eqn (4),[36] where the sharp peak at around 0.02 V corresponds to the Li insertion into amorphous carbon, however, we are unable to identify the de-insertion reaction peak of carbon in our CV result. From the CV results, we can conclude that the overall electrochemical process for the composite materials might involve all four reactions given above.

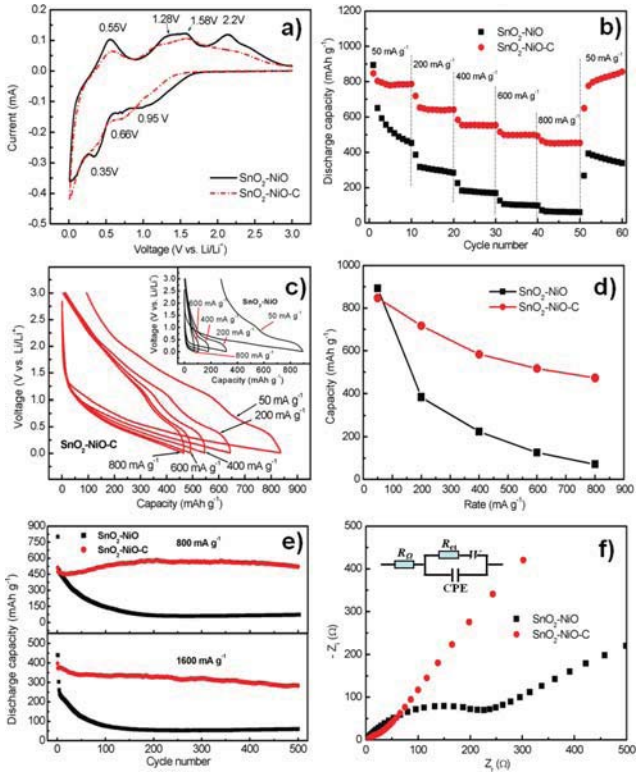

Fig. 4 Electrochemical performances of SnO_2–NiO and SnO_2–NiO–C: (a) cyclic voltammograms at a sweep rate of 0.1 mV s^{-1}; (b) consecutive cyclic behavior at different rates; (c) galvanostatic charge–discharge voltage profiles for SnO_2–NiO–C, with the inset showing comparable profiles for SnO_2–NiO; (d) rate capability at different current densities; (e) cycle life at high current densities of 800 mA g^{-1} and 1600 mA g^{-1}; and (f) EIS spectrum after charge/discharge, with the inset showing the equivalent circuit.

In order to allow full estimation of the electrochemical performance of SnO_2–NiO and SnO_2–NiO–C electrodes, the consecutive cycling behaviours (Fig. 4(b)) and galvanostatic charge–discharge voltage profiles (Fig. 4(c)) at various charge/discharge rates (50, 200, 400, 600, and 800 mA g^{-1}) are shown in Fig. 4. The specific discharge capacity of the SnO_2–NiO–C electrode at 600 mA g^{-1} is 58% of its initial specific discharge capacity at 50 mA g^{-1}. In fact, when discharged at 800 mA g^{-1}, the specific discharge capacity still shows approximately 54% of the first specific capacity that obtained at 50 mA g^{-1}. On returning to 50 mA g^{-1}, the electrode delivers a specific discharge capacity of about 852 mA h g^{-1}, even after 60 cycles. In contrast, the specific discharge capacity of the SnO_2–NiO electrode at 600 mA g^{-1} and 800 mA g^{-1} is only 11% and 7% of its initial specific discharge capacity at 50 mA g^{-1}, respectively. Fig. 4(d) shows the variation in the cell capacity as a function of the applied discharge rate, expressed in mA g^{-1}. The lowest slope indicates the best rate capability. That is to say, the SnO_2–NiO–C electrode shows the best rate capability. Here, the carbon component could increase the electron transfer and reduce the charge transfer resistance within the electrode, giving the carbon coated composite the best rate capability. At the low discharge rate of 50 mA g^{-1}, no differences in specific capacity can be observed for the two electrodes. This is reasonable because Li^+ insertion/extraction is sufficient at the relatively low charge/discharge rate. The specific capacity difference between the SnO_2–NiO and SnO_2–NiO–C electrodes increases with increasing charge/discharge rate. This result confirms that the carbon coating on SnO_2–NiO particles can significantly improve the kinetics of the SnO_2–NiO–C electrode. Fig. 4(e) presents the cycle life up to 500 cycles for both samples at the high discharge rates of 800 mA g^{-1} and 1600 mA g^{-1}. For the SnO_2–NiO electrode, the degradation in the specific discharge capacity is very significant, and this trend can be observed throughout the whole cycling process. However, after carbon coating, the electrochemical properties improved dramatically, and the SnO_2–NiO–C electrode demonstrates a stable specific capacity as high as 529 mA h g^{-1} at 800 mA g^{-1} and 265 mA h g^{-1} at 1600 mA g^{-1}, even after 500 cycles. This

excellent performance is better than those of other Sn-based or Ni based composite materials,[19,34,38] which makes the materials more promising for further investigation for lithium battery applications.

AC electrochemical impedance spectroscopy (EIS) was performed on the SnO_2–NiO and SnO_2–NiO–C composite electrodes, as shown in Fig. 4(f). Prior to the AC impedance testing, the electrodes were cycled galvanostatically for five cycles to ensure the stable formation of the SEI layer on the surface of the electro-active particles. Impedance studies were carried out on the cycled SnO_2–NiO and SnO_2–NiO–C electrodes at the potential of 1.85 and 2.25 V *vs.* Li, respectively. An equivalent circuit (Fig. 4(f), inset) was used for fitting the electrochemical impedance spectra. The intercept at the Z_{real} axis at high frequency corresponds to the ohmic resistance (R_Ω), which represents the total resistance of the electrolyte, separator, and electrical contacts. The semicircle in the middle frequency range indicates the charge transfer resistance (R_{ct}). The inclined line at lower frequency represents the Warburg impedance (W), which is associated with lithium-ion diffusion in the SnO_2–NiO particles. The resistance of the combination of the electrolyte, separator, and electrical contacts (R_Ω) is similar for both electrodes. This is because the electrodes were prepared by adding a conductive carbon black agent, which induces good conductivity in the electrode. It can be clearly seen that the fitted value of R_{ct} is much smaller for the SnO_2–NiO–C electrode ($R_{ct} = 41 \pm 5\ \Omega$) than for the SnO_2–NiO electrode ($R_{ct} = 303 \pm 5\ \Omega$), which indicates that the carbon coating could enable much easier charge transfer at the electrode/electrolyte interface, and consequently decrease the overall battery internal resistance. The electrode could accordingly possess higher reactivity and lower polarization. In other respects, the modifications in impedance are also associated with the component alterations of the electrode. The amorphous carbon layering on the nanoparticles has multiple actions: extending the surface area, preventing aggregation, and enhancing the electronic conductivity of the composite material, which would contribute together to enhance the structural stability, improve the lithium storage kinetics, and stabilize SEI films, resulting in improved rate and cycling performance.

Conclusions

Carbon-coated SnO_2–NiO nanocomposite has been successfully produced by a molten salt method, followed by a carbon layering process. The composite, along with bare SnO_2–NiO, was investigated as anode for lithium-ion batteries. The XRD studies show that the product was a dual phase oxide composed of tetragonal SnO_2 and cubic structure NiO. TEM images of the SnO_2–NiO–C powder indicate that the crystallite sizes of SnO_2 and NiO are in the range of 1–2 nm and 13–90 nm, respectively. The oxide particles were found to be covered by an amorphous carbon layer, and the carbon covered SnO_2 and NiO particles are embedded in a carbon matrix. It was found that the discharge capacity of SnO_2–NiO was dramatically improved after coating with amorphous carbon. The carbon coated composite showed the best electrochemical performance in terms of high capacity, enhanced rate capability, and excellent cycling stability, with capacity of 529 mA h g^{-1} at 800 mA g^{-1} and 265 mA h g^{-1} at 1600 mA g^{-1}, even after 500 cycles. This high performance can be ascribed to the combined effects of the nanosize compound, good interface behavior between the carbon matrix and the SnO_2–NiO structure, and the highly porous nature of the carbon matrix. This research suggests that carbon-coated SnO_2–NiO nanocomposite could be a promising anode material for lithium-ion batteries.

Acknowledgements

The authors would like to thank Dr Tania Silver for critical reading and correction of this manuscript. Mohd Faiz Hassan is grateful to the Ministry of Higher Education of the Government of Malaysia for scholarship support. Financial support from the Australian Research Council (ARC) through project LP0775456 is greatly appreciated.

References

1 Y. G. Guo, J. S. Hu and L. J. Wan, *Adv. Mater.*, 2008, **20**, 2878.
2 C. Masarapu, V. Subramanian, H. Zhu and B. Wei, *Adv. Funct. Mater.*, 2009, **19**, 1008.
3 P. Poizot, S. Laruelle, S. Grugeon, L. Dupont and J. M. Tarascon, *Nature*, 2000, **407**, 496.
4 Y. Yu, Y. Shi and C. Chen, *Nanotechnology*, 2007, **18**, 055706.
5 J. L. Shui, Y. Yu and C. H. Chen, *Appl. Surf. Sci.*, 2006, **253**, 2379.
6 Y. Yu, C. H. Chen and Y. Shi, *Adv. Mater.*, 2007, **19**, 993.
7 Y. Yu, J. L. Shui, S. Xie and C. H. Chen, *Aerosol Sci. Technol.*, 2005, **39**, 276.
8 J. Yang, Y. Takeda, N. Imanishi and O. Yamamoto, *J. Electrochem. Soc.*, 1999, **146**, 4009.
9 L. Wang, S. Kitamura, T. Sonoda, K. Obata, S. Tanase and T. Sakai, *J. Electrochem. Soc.*, 2003, **150**, A1346.
10 J. Wolfenstine, S. Campos, D. Foster, J. Read and W. Behl, *J. Power Sources*, 2002, **109**, 230.
11 H. Shin and M. Liu, *Adv. Funct. Mater.*, 2005, **15**, 582.
12 X. Cheng and P. Shi, *J. Alloys Compd.*, 2005, **391**, 241.
13 J. Hassoun, S. Panero, P. Simon, P. L. Taberna and B. Scrosati, *Adv. Mater.*, 2007, **19**, 1632.
14 L. Shi, H. Li, Z. Wang, X. Huang and L. Chen, *J. Mater. Chem.*, 2001, **11**, 1502.
15 O. Mao and J. R. Dahn, *J. Electrochem. Soc.*, 1999, **146**, 423.
16 F. Chen, Z. Shi and M. Liu, *Chem. Commun.*, 2000, **21**, 2095.
17 Y. Wang, J. Y. Lee and T. C. Deivaraj, *J. Electrochem. Soc.*, 2004, **151**, A1804.
18 F. Belliard and J. T. S. Irvine, *J. Power Sources*, 2001, **97–98**, 219.
19 S. H. Choi, J. S. Kim and Y. S. Yoon, *Electrochim. Acta*, 2004, **50**, 547.
20 R. K. Selvan, N. Kalaiselvi, C. O. Augustin, C. H. Doh and C. Sanjeeviraja, *J. Power Sources*, 2006, **157**, 522.
21 Y. Liang, J. Fan, X. H. Xia, Y. S. Luo and Z. J. Jia, *Electrochim. Acta*, 2007, **52**, 5891.
22 C. Li, W. Wei, S. Fang, H. Wang, Y. Zhang, Y. Gui and R. Chen, *J. Power Sources*, 2010, **195**, 2939.
23 J. Hassoun, S. Panero, G. Mulas and B. Scrosati, *J. Power Sources*, 2007, **171**, 928.
24 H. Guo, H. Zhao and X. Jia, *Electrochem. Commun.*, 2007, **9**, 2207.
25 M. Wojciechowska, M. Zielinski, A. Malczewska, W. Przystajko and M. Pietrowski, *Appl. Catal., A*, 2006, **298**, 225.
26 P. Lavela and J. L. Tirado, *J. Power Sources*, 2007, **172**, 379.
27 P. Lavela, J. L. Tirado and C. Vidal-Abarca, *Electrochim. Acta*, 2007, **52**, 7986.
28 Z. P. Guo, G. D. Du, Y. Nuli, M. F. Hassan and H. K. Liu, *J. Mater. Chem.*, 2009, **19**, 3253.
29 W. Tang, X. Yang, Z. Liu, S. Kasaishi and K. Ooi, *J. Mater. Chem.*, 2002, **12**, 2991.
30 J. D. Pateris and B. Wopenka, *Astrobiology*, 2003, **3**, 727.
31 C. J. Yang, J. L. Jiang, D. J. Ping and Z. H. Fei, *Chin. Phys. Lett.*, 2008, **25**, 780.
32 A. Guedes, N. Ribeiro, M. Oliveira, F. Noronha and I. Abreu, *J. Aerosol Sci.*, 2009, **40**, 81.

33 X. H. Huang, J. P. Tu, C. Q. Zhang and J. Y. Xiang, *Electrochem. Commun.*, 2007, **9**, 1180.
34 M. M. Rahman, S. L. Chou, C. Zhong, J. Z. Wang, D. Wexler and H. K. Liu, *Solid State Ionics*, 2010, **180**, 1646.
35 P. A. Connor and J. T. S. Irvine, *J. Power Sources*, 2001, **97–98**, 223.
36 J. Yao, X. Shen, B. Wang, H. Liu and G. Wang, *Electrochem. Commun.*, 2009, **11**, 1849.
37 M. Mohamedi, S. J. Lee, D. Takahashi, M. Nishizawa, T. Itoh and I. Uchida, *Electrochim. Acta*, 2001, **46**, 1161.
38 Y. N. Li, P. Zhang, Z. Guo, H. K. Liu, J. Yang and J. Wang, *Mater. Res. Bull.*, 2009, **44**, 140.

